Research Paper https://doi.org/10.7733/jnfcwt.2024.024

Solubility of Trivalent Am, Eu, and Sm in the Synthetic KAERI Underground Research Tunnel Groundwater

Hee-Kyung Kim*, Hye-Ryun Cho, and Wansik Cha
Korea Atomic Energy Research Institute, 111, Daedeok-daero 989beon-gil, Yuseong-gu, Daejeon 34057, Republic of Korea

(Received March 27, 2024 / Revised April 15, 2024 / Approved May 20, 2024)

The initial radionuclide migration quantity depends on the total amount of solubilized species. Geochemical modeling based on a thermodynamic database (TDB) has been employed to assess the solubility of radionuclides. It is necessary to evaluate whether the TDB describes the domestic repository conditions appropriately. An effective way to validate the TDB-based modeling results is through direct comparisons with experimentally measured values under the conditions of interest. Here, the solubilities of trivalent Sm, Eu, and Am were measured in synthetic KURT-DB3 groundwater (Syn-DB3) and compared with modeling results based on ThermoChimie TDB. $Ln_2(CO_3)_3 \cdot xH_2O$(cr) (Ln = Sm, Eu) solids were introduced into the Syn-DB3 and dissolved Sm and Eu concentrations were monitored over 223 days. X-ray diffraction analysis confirmed that the crystallinity of the solid compounds was maintained throughout the experiments. The dissolved Sm and Eu concentrations at equilibrium were close to the predicted solubilities of $Sm_2(CO_3)_3$(s) and $Eu_2(CO_3)_3$(s) based on the ThermoChimie TDB. The Am solubility measured under oversaturated conditions was comparable to the measured Eu concentrations, although they were measured under different experimental settings. More experimental data are needed for Am-carbonate solid systems with careful characterization of the solid phases to better evaluate Am solubility in domestic groundwater conditions.

Keywords: Trivalent americium, Trivalent lanthanide, Solubility, KURT groundwater, Radionuclide migration, Thermodynamic database

*Corresponding Author.
Hee-Kyung Kim, Korea Atomic Energy Research Institute, E-mail: hkim11@kaeri.re.kr, Tel: +82-42-866-6294

ORCID
Hee-Kyung Kim http://orcid.org/0000-0001-5840-7194
Hye-Ryun Cho http://orcid.org/0000-0002-1293-6653
Wansik Cha http://orcid.org/0000-0001-6153-1647

This is an Open-Access article distributed under the terms of the Creative Commons Attribution Non-Commercial License (http://creativecommons.org/licenses/by-nc/3.0) which permits unrestricted non-commercial use, distribution, and reproduction in any medium, provided the original work is properly cited

1. Introduction

Radionuclide migration through the underground multibarrier repository system of high-level radioactive waste (HLW) and transportation to the ecosystem should be thoroughly understood to evaluate the proof-of-safety of the repository system [1]. Groundwater flow is a major route of radionuclide migration, and the migration quantity depends on the total amount of solubilized radionuclides [2]. It is difficult to experimentally assess nuclide solubility under vast variations in spatiotemporal conditions. Geochemical modeling based on a thermodynamic database (TDB) has been employed to evaluate the solubility under diverse repository conditions [3].

The complex formation of radionuclides with groundwater components determines the solubility of radionuclide compounds and directly affects sorption and diffusion through engineered and natural barriers [4, 5]. The oxidation state of a radionuclide is an important factor affecting its chemical reactivity. Ideally, all possible chemical processes including aqueous chemical reactions, solid-phase dissolution, and redox reactions should be considered. The reliability of geochemical modeling depends on the accuracy of the thermodynamic data and the comprehensiveness of the TDB. An effective way to validate a TDB, that is, whether it can describe domestic conditions appropriately, is to directly compare the modeling results with the experimentally measured values.

In our previous study, Am solubility was measured in synthesized groundwater (Syn-DB3) by simulating groundwater conditions at the DB3 site in the KAERI underground research tunnel (KURT) [6]. Due to the shortage of Am in stock to prepare solid phases, the experiment was conducted under oversaturation conditions, where aqueous Am (^{241}Am, $t_{1/2}$ = 432.7 years) [7] was added to Syn-DB3, and the Am concentration in the supernatant was monitored using LSC. In this study, three main issues were identified: 1) The precipitated solids in the samples were not visible and thus could not be characterized. Solid-phase characterization before and after the solubility measurements is important for evaluating the experimental results. 2) The pH values of the samples were not checked at the end of the experiments despite the probable pH changes over a period of long reaction time. 3) The supernatant contained colloidal particles, which would have resulted in overestimation of the dissolved Am concentrations. More rigorous phase separation should be employed to exclude colloidal contributions to the dissolved Am concentrations.

In the thermodynamic studies of aqueous species, Nd(III) and Eu(III) are widely used as nonradioactive analogs of Am(III). The chemical behavior of trivalent actinide (An) and lanthanide (Ln) ions is highly correlated with their ionic radii [8, 9]. Am^{3+} (1.10 Å), Cm^{3+} (1.09 Å), Nd^{3+} (1.11 Å), and Eu^{3+} (1.07 Å) ions have similar ionic radii [8, 10] and differences between their activities in aqueous solutions are often less than the experimental errors [2, 11]. The NEA-TDB project has used these analogies to evaluate the thermodynamics of aqueous Am(III) species using experimental data for Cm(III), Nd(III) and Eu(III) [2, 12]. Notably, the solubility properties of the isostructural solids of Am(III) and Ln(III) can differ considerably, unlike in aqueous chemistry. Even in these cases, the NEA-TDB project discussed the solubility constants of Am(III) solids in comparison with those of isostructural Ln(III) solids, as Ln are free from alpha-radiation damage and theirs crystallinities can be relatively well characterized [2, 12].

The present study aimed to measure solubility of Ln(III) compounds of $Ln_2(CO_3)_3 \cdot xH_2O$(cr) (Ln = Sm, Eu) in the Syn-DB3 in under-saturation conditions. Eu was employed as the nonradioactive analog of Am. Sm was also examined because it is a trivalent Ln element included in the safety assessments of the HLW repository system conducted by the Institute for Korea Spent Nuclear Fuel (iKSNF) [13]. The solid compounds were characterized by x-ray diffraction (XRD) before and after the solubility study. Ultrafiltration was used to separate the dissolved metal ions from the solid phase. The pH and composition of the samples were analyzed at the end of the experiment. The aqueous

Table 1. Physicochemical properties of the Syn-DB3 before and after experiments

Element		Syn-DB3	After Sm experiment	After Eu experiment
	pH	9.03	8.19	8.26
	Eh (V)	0.436	Not measured	Not measured
Chemical composition ($mg \cdot L^{-1}$)	Na	38.2	38.9	39.0
	Ca	5.3	4.9	5.0
	K	0.48	0.52	0.52
	Mg	0.26	0.28	0.29
	HCO_3	84.13	83.0	82.9
	SiO_2	7.7	7.8	7.70
	Cl	1.76	1.80	1.79
	SO_4	5.51	5.49	5.55
	F	7.67	7.73	7.82

Table 2. Sm and Eu solubility samples

Sample	Added solid (mg) in 500 mL Syn-DB3	Added $[Ln]_{total}$ (M)	Measured $[Ln]_{supernatant}$ (M)	Measured $[Ln]_{UF}$ (M)
Sm1	59.4	4.9×10^{-4}	$(6.21 \pm 0.12) \times 10^{-8}$	$(3.98 \pm 0.04) \times 10^{-8}$
Sm2	54.9	4.6×10^{-4}		
Sm3	66.3	5.5×10^{-4}		
Eu1	64.8	5.4×10^{-4}	$(8.84 \pm 0.28) \times 10^{-8}$	$(6.08 \pm 0.05) \times 10^{-8}$
Eu2	58.1	4.8×10^{-4}		
Eu3	53.7	4.4×10^{-4}		

Eu(III) species were investigated using time-resolved laser-induced fluorescence spectroscopy (TRLFS). For comparison, the solubility of Am in Syn-DB3 was also measured under oversaturated conditions in continuation of the previous study [6]. The measured solubility values were compared with geochemical modeling results based on ThermoChimie (ver. 11a) TDB [14].

2. Experimental

2.1 $Ln_2(CO_3)_3 \cdot xH_2O$ Solubility Sample Preparations: Under-Saturation Conditions

Solid reagents of $Sm_2(CO_3)_3 \cdot xH_2O$ and $Eu_2(CO_3)_3 \cdot xH_2O$ (Alfa Aesar, REacton 99.99%) were used as purchased. Syn-DB3 was prepared as described previously [6] and its composition is listed in Table 1. Syn-DB3 is an oxidative groundwater (Eh = 0.436 V) at pH 9.03. Samples for solubility measurements were prepared by adding solid powders to 500 mL of Syn-DB3 groundwater (PE 500 mL bottles). Three Sm repeats contained 59.4, 54.9, and 66.3 mg of $Sm_2(CO_3)_3 \cdot xH_2O$ powder and three Eu repeats contained 64.8, 58.1, and 53.7 mg of $Eu_2(CO_3)_3 \cdot xH_2O$ powder (Table 2). These values were more than 10^4 times higher than the expected solubility values.

2.2 Determination of Dissolved Sm and Eu Concentration

Concentrations of Sm and Eu in the supernatant of the test samples were periodically measured; 10 mL of

the supernatant was sampled from the top of the samples, mixed with 100 μL of high-purity HNO_3 (13.14 M, Ultrapur, Merck) in 10 mL centrifuge tubes, and sent for analysis using inductively coupled plasma-mass spectrometry (ICP-MS). Samples were collected at 2 h, 1 day, 7 days, 20 days, 50 days, 90 days, and 223 days.

At the end of the experiments, when no further concentration changes were observed, the final Sm and Eu concentrations were analyzed after phase separation using an ultrafiltration device (10 kDa, Amicon Ultra-15 centrifugal filter, Millipore), after which, 10 mL of the supernatant was placed in an ultrafiltration device, centrifuged (5,000 rpm, 1 h), and the filtrate was transferred to a new falcon tube containing HNO_3 for ICP-MS analysis. This process was repeated four times, and the concentrations of Sm and Eu in each filtrate were analyzed using ICP-MS.

2.3 Characterizations of Residual Solids and Aqueous Phases at the end of the Experiments

At the end of the solubility measurements, the supernatants of the Sm and Eu samples were analyzed for pH and concentrations of the main components using ICP-optical emission spectrometry. After 223 days of solubility testing, the solid phase that had settled to the bottom of the solution was filtered through a membrane filter (0.2 μm), air dried, and subjected to XRD analysis.

2.4 TRLFS of Eu Solution

The Eu filtrates (0.2 μm) at the end of the solubility measurements were analyzed by time-resolved laser induced fluorescence spectroscopy (TRLFS) [15, 16]. Briefly, a nanosecond-pulsed wavelength-tunable OPO laser system (Opotek Inc. Vibrant B) was used as the excitation source at 394 nm (1.1 mJ). Luminescence spectra was measured using an intensified CCD (ICCD) detector via a spectrograph with a slit width of 300 μm and grating of 300 lines·mm^{-1} (Andor Technol. SR-303i). Samples were incubated at 25°C in quartz cuvettes during the measurements. Luminescence decay rates were measured using a kinetic mode of the ICCD detection with a gate width of 1 ms, initial gate opening delay of 1 μs, and stepwise delay by 30 μs. The number of hydration ($n(H_2O)$) in inner-sphere of Eu(III) center was calculated according to the relation with the decay lifetime (τ) as described in Equation (1) [17, 18].

$$n(H_2O) \pm 0.5 = 1.07/\tau\ (ms) - 0.62 \quad (1)$$

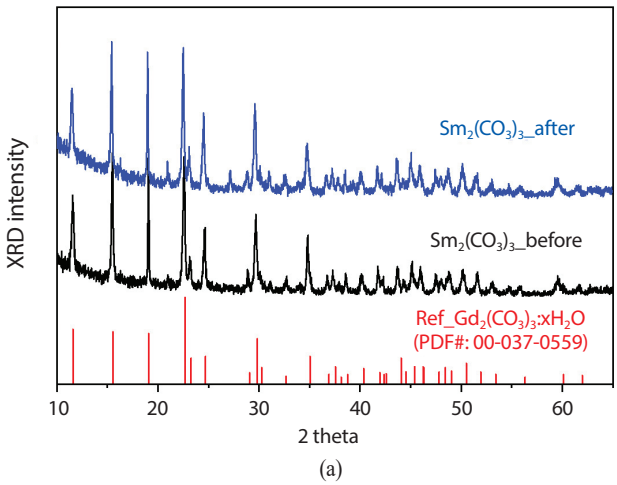
2.5 Am Solubility Measurements: Over-Saturation Conditions

Am sample preparation was described in previous study [6]. Briefly, a series of pH-varied Am(III) samples (11.8 μM) were prepared in Syn-DB3. pH values of the samples were adjusted to be in the range of 6.4–10 by adding 0.2 M $HClO_4$ (ULTREX II, Ultrapure reagent, JT Baker) or 0.1 M NaOH (Semiconductor grade, 99.99% trace metals basis, Sigma-Aldrich). Two milliliters of each sample were stored in quartz cells with a screw cap, and their absorption spectra were monitored periodically. Absorption data between 0–70 days were already reported in our previous study [6]. In this study, the samples were kept unopened until the last day of the experiments (231 days), when the samples were subjected to pH and Am concentration analyses. Phase-separation was conducted using ultrafiltration (10 kDa, Amicon Ultra-0.5 centrifugal filter, Millipore) and the fourth filtrates were analyzed by LSC. Detailed experimental conditions for LSC radiometry are described in our previous study [6].

3. Results and Discussion

3.1 XRD Analysis on $Ln_2(CO_3)_3 \cdot xH_2O$ Before and After Experiments

$Ln_2(CO_3)_3 \cdot xH_2O$ (Ln = Sm, Eu) powders were analyzed



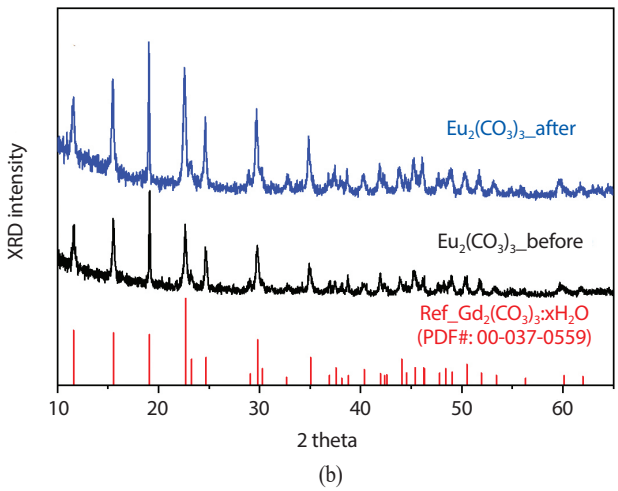
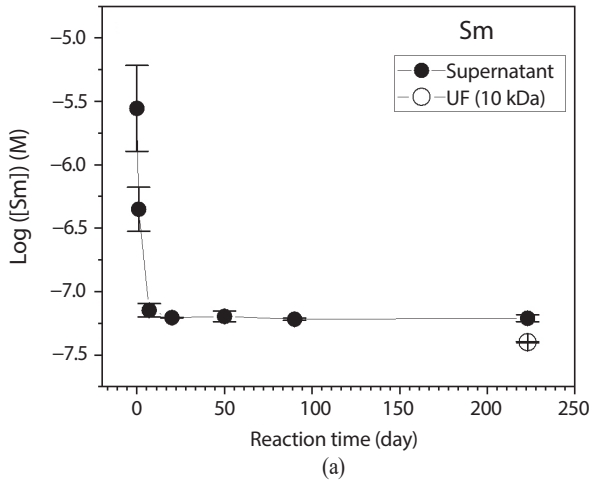


Fig. 1. XRD patterns of the (a) Sm and (b) Eu solids before (black) and after (blue) solubility measurements. Red is XRD pattern of $Gd_2(CO_3)_3{\cdot}xH_2O$ (PDF #: 00-037-0559).



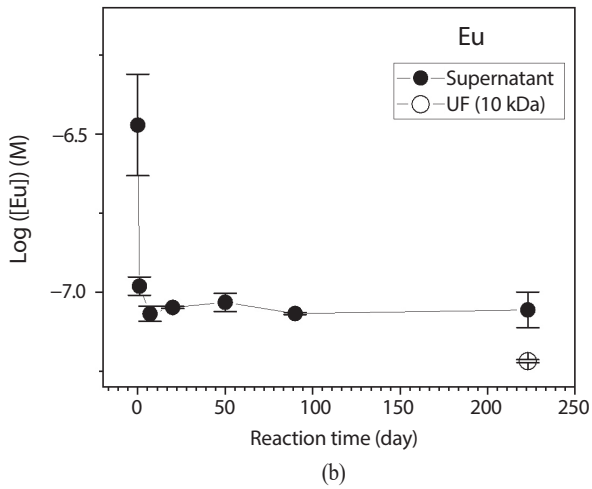


Fig. 2. Solubility of (a) Sm and (b) Eu in the Syn-DB3 groundwater. Closed and open circles are concentrations in supernatant before and after ultrafiltration (UF), respectively.

by XRD before experiments. The measured patterns shown in Fig. 1 are almost identical to that of the crystalline $Gd_2(CO_3)_3{\cdot}xH_2O$(cr) (PDF#: 00-037-0559, orthorhombic). These results indicate that the Sm and Eu powders are crystalline, similar to the $Gd_2(CO_3)_3{\cdot}xH_2O$(cr).

After solubility measurements, the collected residual solid phases were analyzed using XRD. The XRD patterns of the solid phases before and after the tests were the same for Sm and Eu, as shown in Fig. 1. The results showed that the crystal structures of the Sm and Eu powders were maintained in the solutions during the solubility experiments.

3.2 Solubility of Sm and Eu

The results of the dissolved Sm and Eu concentration analyses are listed in Table 2. The dissolved Sm concentration reached equilibrium on reaction day of 20 and remained constant until the end of the experiment (day 223) (Fig. 2 (a)). The average Sm concentration in the supernatant during 20–223 days was $(6.21 \pm 0.12)\times10^{-8}$ M. Similarly, Eu concentration reached equilibrium on day 7 and the average Eu concentration in the supernatant during 7–223 days was $(8.84 \pm 0.28)\times10^{-8}$ M.

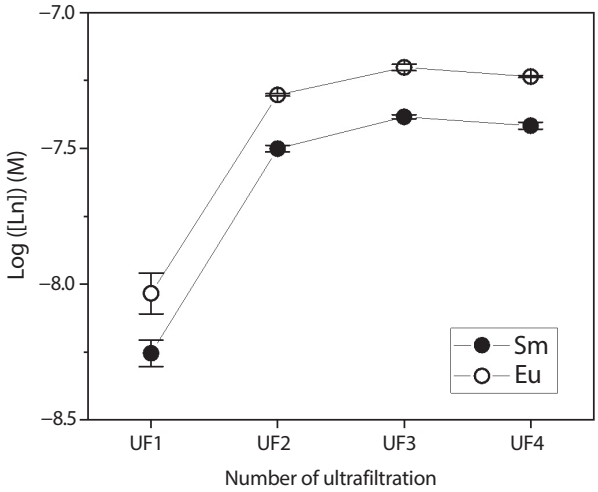


Fig. 3. Sm and Eu ion concentrations in the filtrates depending on the number of ultrafiltration.

Once the samples were confirmed to be in equilibrium, the supernatants were subjected to ultrafiltration (10 kDa) for phase separation on the last day of the experiment (Day 223). A single membrane filter unit was used for repeated filtration four times (UF1–UF4) for each sample, and the Sm and Eu concentrations were tracked as the filtration was repeated. The Sm and Eu concentrations in the filtrates increased significantly from the first (UF1) to the second round (UF2) of filtration and leveled off after UF2 (Fig. 3). The low concentrations in the first two filtrates were ascribed to the adsorption of metal ions on the membrane filters and the vessel surface. After UF2, no considerable changes in the Sm and Eu concentrations were observed, indicating that the adsorption sites of the filtration unit were saturated after two rounds of filtration.

The mean values of Sm and Eu concentrations in each of UF3 and UF4 were $(3.98 \pm 0.04)\times10^{-8}$ M and $(6.08 \pm 0.05)\times10^{-8}$ M, respectively. These values were slightly lower than those measured without phase separation (Fig. 2 and Table 2). The pH of the Sm and Eu samples at the end of the experiments was 8.19 and 8.26, respectively. These values were lower than those obtained under the initial Syn-DB3 conditions (pH 9.03). No significant changes in the concentrations of the main components were detected after the experiment (Table 1). The carbonate content estimated from alkalinity was maintained until the end of the experiment.

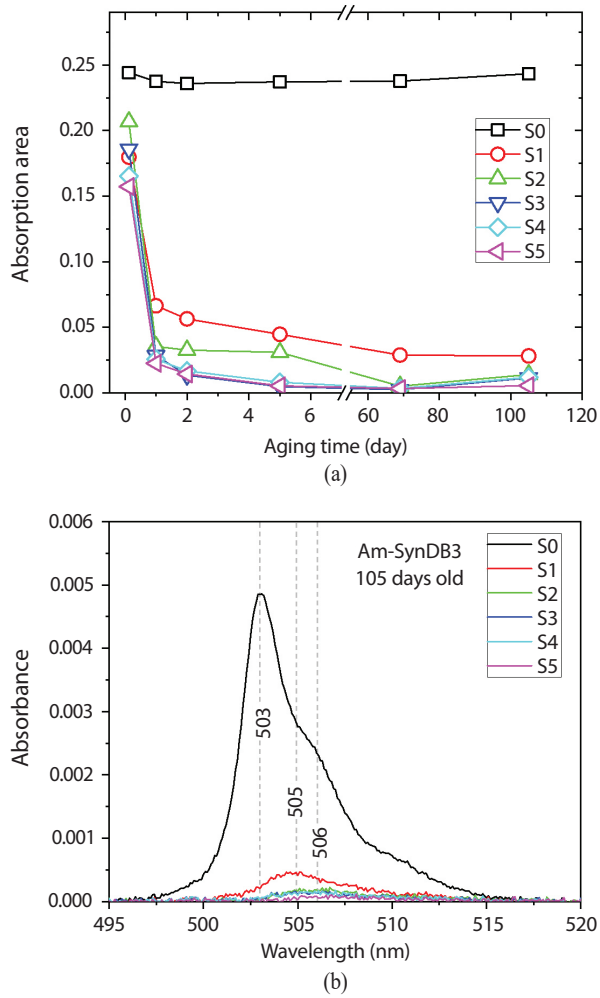


Fig. 4. Absorption properties of Am(II) in the Syn-DB3 samples.
(a) Aging time-dependent absorption area changes of the samples. Data of 0–70 days are the same as in previous study [6].
(b) Absorption spectra of the samples in 105 days.

3.3 Am Solubility Tested in Over-Saturation Experiments

The absorption spectra of the Am samples stored in quartz cuvettes were periodically measured to monitor their equilibrium status. The absorption data for the first 70 days in Fig. 4(a) were already reported in our previous study [6].

Table 3. Am solubility samples in cuvettes

Am in Syn-DB3	Initial pH	Final pH (231 d)	$[Am]_{UF}$ (231 d) (M)
S0	1	1	Not measured
S1	6.38	7.27	2.70×10^{-7}
S2	7.50	8.30	6.34×10^{-8}
S3	8.36	8.48	3.58×10^{-8}
S4	8.71	8.56	6.39×10^{-8}
S5	10.5	10.1	2.05×10^{-8}

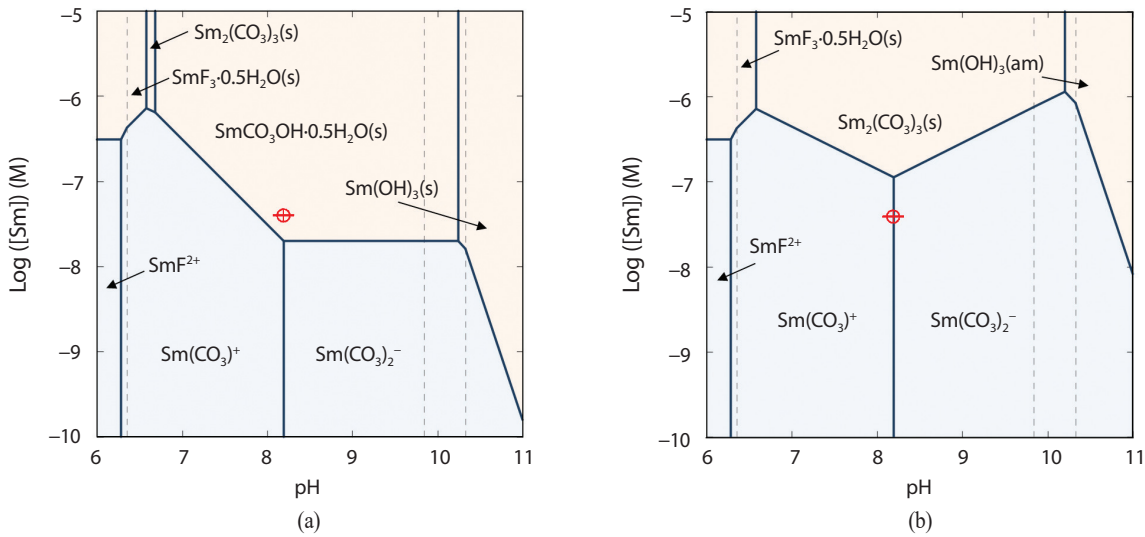


Fig. 5. Solubility curves and aqueous species of Sm in the Syn-DB3. ThermoChimie 11a TDB was used as an input database with (a) excluding formation of $SmCO_3OH(cr)$ and (b) additionally excluding formation of $SmCO_3OH{\cdot}0.5H_2O(s)$, and $Sm(OH)_3(s)$. Open red circle is experimentally determined dissolved Sm concentration at pH 8.19 after ultrafiltration.

The absorption spectrum of the reference sample (pH 1 in Fig. 4) was consistent throughout the experiment. However, all the samples in the Syn-DB3 showed a significant decrease in absorbance in one day, after which a gradual decrease in absorbance was observed for 70 days, as shown in Fig. 4(a). No peak shifts were observed, as described in our previous study [6]. The absorption spectra of samples at 105 days are presented in Fig. 4(b). The results showed that the Am samples in Syn-DB3 reached equilibrium in 70 days, during which most of the Am precipitated. The absorbance at 505–506 nm was likely due to colloidal Am(III) compounds that are not luminescent, as discussed previously [6].

As no further change in absorbance was confirmed, the samples in the cuvettes were opened to analyze the pH and aqueous Am concentrations on reaction day 231. The results are summarized in Table 3. In comparison to the initial pH values, all the samples showed changes in pH values. The aqueous Am concentrations were measured after phase separation by ultrafiltration (10 kDa). In general, the Am concentration in the filtrates decreased as pH increased. In the range of pH 8–9 (8.45 ± 0.13 on average of S2−4), the averaged aqueous Am concentration was $(5.48 \pm 1.3)\times10^{-8}$ (Table 3), which was in the same range as the dissolved Eu concentration ($(6.08 \pm 0.05)\times10^{-8}$ M, Table 2) at pH 8.26.

Table 4. Thermodynamic data of trivalent Sm, Eu, and Am in ThermoChimie 11a

Reaction	log$K°$(Sm)	log$K°$(Eu)	log$K°$(Am)
$MCO_3OH(cr) + H^+ \rightleftarrows M^{3+} + CO_3^{2-} + H_2O$	−10.23 ± 0.65	−9.63 ± 0.80	−11.51 ± 1.14
$MCO_3OH{:}0.5H_2O(s) + H^+ \rightleftarrows M^{3+} + CO_3^{2-} + 1.5H_2O$	−7.31 ± 0.72	−7.80 ± 1.15	−8.4 ± 0.50*
$MCO_3OH(s) + H^+ \rightleftarrows M^{3+} + CO_3^{2-} + H_2O$	-	-	−6.2 ± 1.00*
$M_2(CO_3)_3(s) \rightleftarrows 2M^{3+} + 3CO_3^{2-}$	−34.50 ± 2.00**	−35.00 ± 3.25**	−33.4 ± 2.20*
$M(OH)_3(cr) + 3H^+ \rightleftarrows M^{3+} + 3H_2O$	-	15.46 ± 1.00	15.6 ± 0.60*
$M(OH)_3(s) + 3H^+ \rightleftarrows M^{3+} + 3H_2O$	16.13 ± 1.00	-	-
$M(OH)_3(am) + 3H^+ \rightleftarrows M^{3+} + 3H_2O$	17.85 ± 1.01	17.6 ± 0.84	16.9 ± 0.80*
$M^{3+} + CO_3^{2-} \rightleftarrows M(CO_3)^+$	7.80 ± 0.50	7.90 ± 0.50	7.90 ± 0.40*
$M^{3+} + 2CO_3^{2-} \rightleftarrows M(CO_3)_2^-$	12.80 ± 0.60	12.9 ± 0.70	12.60 ± 0.60*
$M^{3+} + 3CO_3^{2-} \rightleftarrows M(CO_3)_3^{3-}$	14.80 ± 0.58	14.8 ± 0.58	14.60 ± 1.00*

*Selected in NEA-TDB [12] with crystallinity as $AmCO_3OH{:}0.5H_2O(s) \rightarrow (cr)$, $AmCO_3OH(s) \rightarrow (am,hyd)$, $Am_2(CO_3)_3(s) \rightarrow (am)$
** Crystallinity not identified, but assumed as hydrated crystalline phases according to the synthesis protocol [20]

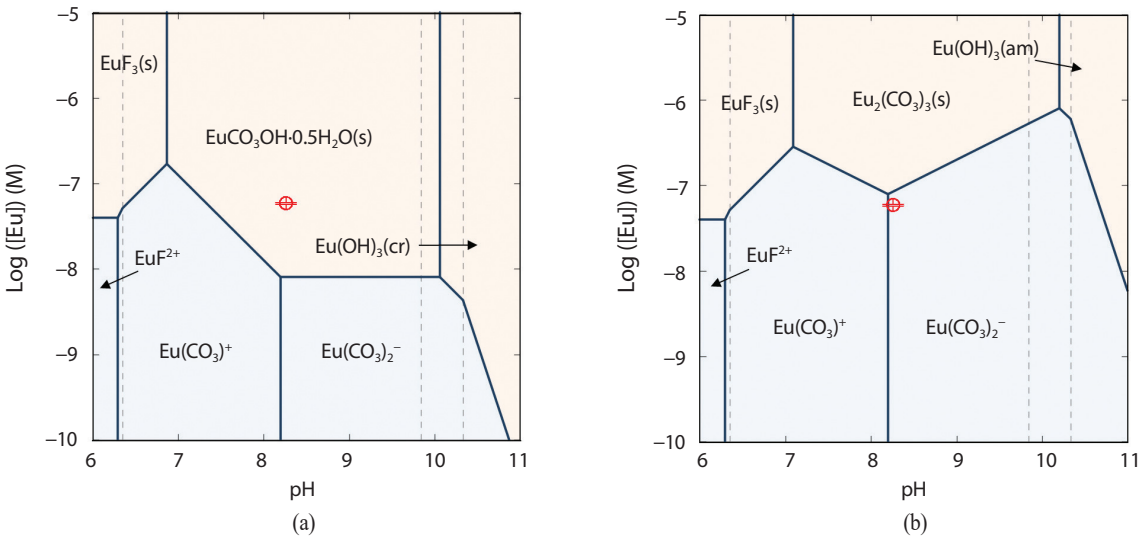


Fig. 6. Solubility curves and aqueous species of Eu in the Syn-DB3. ThermoChimie 11a TDB was used as an input database with (a) excluding formation of $EuCO_3OH(cr)$ and (b) additionally excluding formation of $EuCO_3OH{\cdot}0.5H_2O(s)$, and $Eu(OH)_3(s)$. Open red circle is experimentally determined dissolved Eu concentration at pH 8.26 after ultrafiltration.

3.4 Comparisons Between Geochemical Modeling and Experimental Results

Geochemical modeling of Sm and Eu solubility was performed under the Syn-DB3 conditions determined at the end of the experiments. The Geochemist workbench program (2023 standard) was used with the ThermoChimie (ver. 11a) TDB as primary input data [14]. Modeling was conducted by excluding low-solubility solid phases in a stepwise manner to approach the measured solubility values.

Solubility curves of Sm. Fig. 5 shows the solubility curve of Sm modeled under Syn-DB3 conditions at the

end of the solubility test (see Table 1). After excluding crystalline $SmCO_3OH$(cr), with extremely low solubility, $SmCO_3OH{\cdot}0.5H_2O$(s) was predicted as the solubility-limiting solid phase (Fig. 5(a)). When $SmCO_3OH{\cdot}0.5H_2O$(s) and $Sm(OH)_3$(s) were additionally excluded, $Sm_2(CO_3)_3$(s) was predicted as the solubility-limiting solid phase (Fig. 5(b)).

The dissolved Sm concentration after phase separation was $(3.98 \pm 0.004) \times 10^{-8}$ M, as depicted in the solubility curve (open red circle). It is located in between the predicted concentrations of $SmCO_3OH{\cdot}0.5H_2O$(s) and $Sm_2(CO_3)_3$(s) based on ThermoChimie TDB. In particular, it is slightly lower (by less than 0.5 log unit) compared to the solubility of $Sm_2(CO_3)_3$(s).

The K_{sp} of $Sm_2(CO_3)_3$(s) (-34.50 ± 2.00, see Table 4 for the reaction) in ThermoChimie TDB was adopted from SKB TR 95-35 [19], in which the K_{sp} was evaluated mainly based on experimental results by Firsching and Mohammadzadel [20]. In their work, $Sm_2(CO_3)_3$(s) solid compounds were prepared via decomposition of rare-earth trichloroacetates. Crystalline rare-earth carbonates have been produced using this method [21]. However, the authors did not characterize the solid phases before or after the experiments. The same process was applied to $Eu_2(CO_3)_3$(s), as described in the next section. Considering the uncertainty of the reported K_{sp} of $Sm_2(CO_3)_3$(s) with unidentified crystallinity, the slightly lower solubility for the crystalline $Sm_2(CO_3)_3{\cdot}xH_2O$(cr) compound used in this work is reasonable.

Solubility curves of Eu and aqueous species. Fig. 6 shows the solubility curves of Eu modeled under the Syn-DB3 groundwater conditions at the end of the solubility test (see Table 1). When crystalline $EuCO_3OH$(cr), with extremely low solubility, was excluded, $EuCO_3OH{\cdot}0.5H_2O$(s) was predicted as the solubility-limiting solid phase (Fig. 6(a)). When $EuCO_3OH{\cdot}0.5H_2O$(s) was additionally excluded, $Eu_2(CO_3)_3$(s) was predicted as the solubility-limiting solid phase (Fig. 6(b)). The dissolved Eu concentration after ultrafiltration was $(6.08 \pm 0.05) \times 10^{-8}$ M), as depicted with open red circle on the solubility curve in Fig. 6. The measured Eu concentration was 10 times higher than the

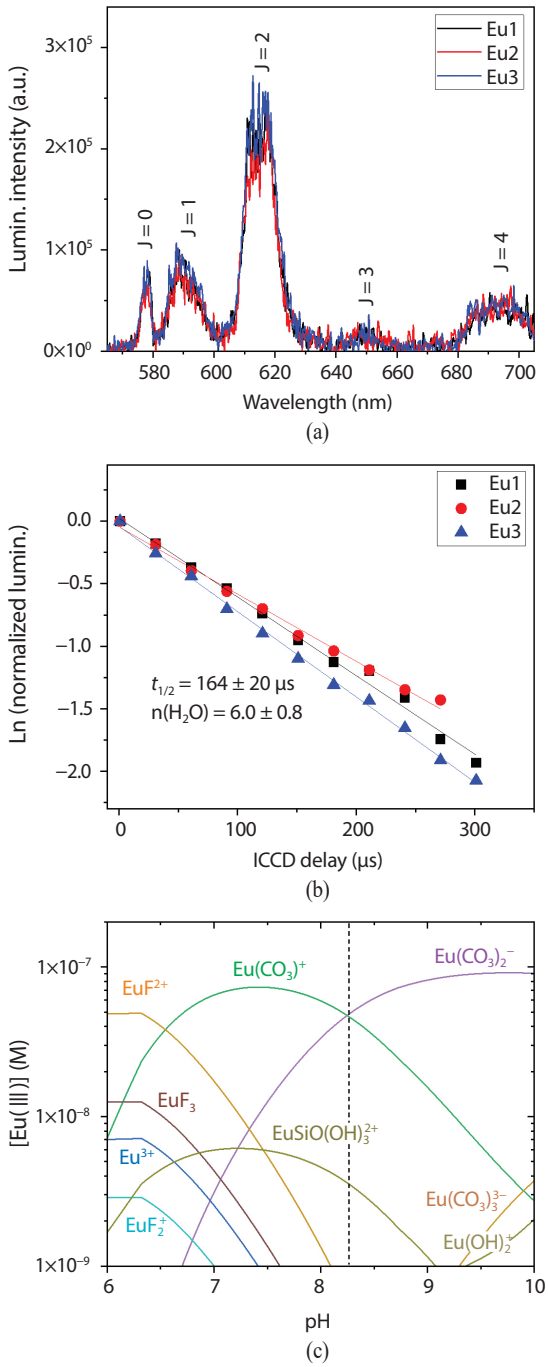


Fig. 7. Aqueous Eu(III) species properties. (a) Representative luminescence spectra of Eu filtrates. They correspond to electronic transitions of $^5D_0 \rightarrow {}^7F_J$ (J = 0–4). (b) Luminescence decays as a function of ICCD delay time. Lifetimes were determined from inverse of the slopes and the inner-sphere hydration number, n(H_2O), was calculated from the lifetime according to equation (1). (c) pH-dependent aqueous Eu(III) species distributions under Syn-DB3 condition based on ThermoChimie TDB. The dotted line is at pH 8.26, the final pH value of the Eu solubility samples.

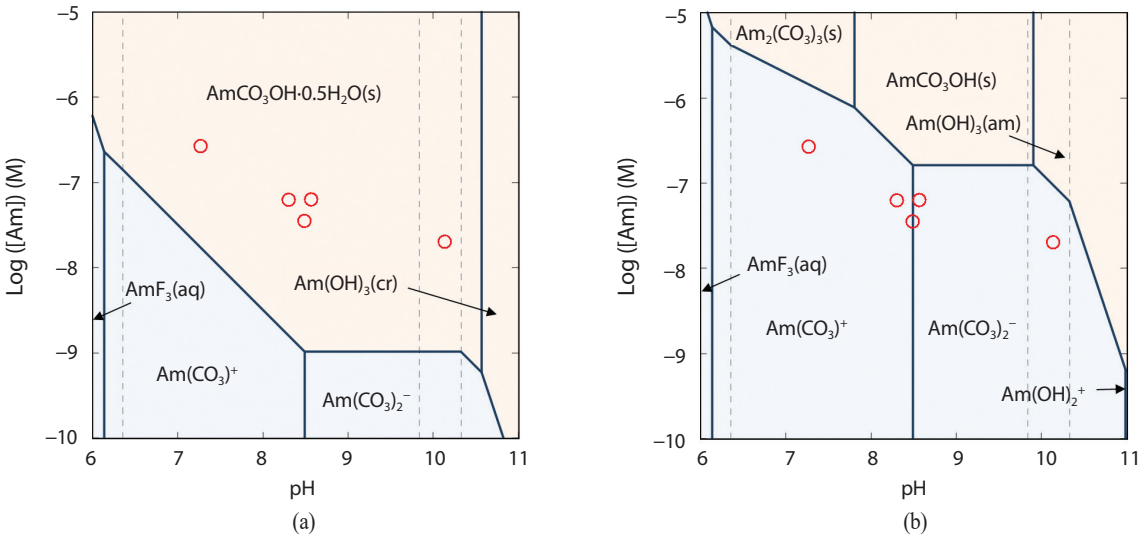


Fig. 8. Solubility curves of Am(III) in Syn-DB3 groundwater condition. ThermoChimie 11a TDB was used as an input database with (a) excluding formation of crystalline $AmCO_3OH$(cr) and (b) additionally excluding crystalline $AmCO_3OH{\cdot}0.5H_2O$(s) and $Am(OH)_3$(cr). Open red circles are experimentally determined dissolved Am concentrations after ultrafiltration.

predicted concentration by $EuCO_3OH{\cdot}0.5H_2O$(s) based on ThermoChimie TDB. The experimental results obtained with crystalline $Eu_2(CO_3)_3{\cdot}xH_2O$(cr) compound here closely follow the K_{sp} of $Eu_2(CO_3)_3$(s) in ThermoChimie, although the ThermoChimie-selected K_{sp} of $Eu_2(CO_3)_3$(s) (−35.00 ± 3.25) has the same issue regarding the unidentified solid phase as described for the case of Sm [19, 20].

As Eu(III) shows strong luminescence properties, the filtered Eu solutions (0.2 μm filter) after the last solubility measurements were examined using TRLFS. Fig. 7 shows the luminescence spectra of the Eu(III) samples and their intensity decay rates. These spectra correspond to the $^5D_0$–^7F_J (J = 0–4) electronic transitions of Eu(III) [22, 23]. All three samples exhibited the same luminescence spectra, where the J = 2 peak, which is a hypersensitive peak, was significantly enhanced relative to the J = 1 peak. The strength of the hypersensitive peak was highly sensitive to inner-sphere environmental changes in the Eu(III) center [22]. Additionally, the appearance of the J = 0 peak is indicative of a low-symmetry Eu (III) site due to complex formation. These spectral properties are well-known features of strongly complex Eu ions [16, 23].

The geochemical modeling results assess that $Eu(CO_3)^+$ and $Eu(CO_3)_2^-$ complexes are the main species in Syn-DB3 at pH 8.26 and they are equally distributed (Fig. 7(c)). The observed luminescence spectral properties are similar to those reported for Eu-CO_3 complexes [24, 25]. The luminescence decay lifetime (τ) was 164 ± 20 μs on average (Fig. 7(b)). According to Equation (1), the inner-sphere hydration number was 6.0 ± 0.8. We considered nine coordination numbers around the Eu(III) center [22, 23]. These results indicate that on average, three water molecules are displaced from the Eu(III) center under the Syn-DB3 condition. The results are in line with the modeling results; mixture of equal amount of $Eu(CO_3)^+$ and $Eu(CO_3)_2^-$ would result in displacing three water molecules on average, as carbonate is typically a bidentate ligand [25].

Solubility curves of Am. Fig. 8 shows the solubility curves of Am modeled under Syn-DB3 groundwater conditions. As the compositions of Syn-DB3 could not be measured after solubility measurements owing to the shortage of samples, modeling was conducted with the initial Syn-DB3 condition. For Sm and Eu, the solution conditions did not significantly change at the end of the experiment.

The $AmCO_3OH$ compounds (crystalline, hydrated, and amorphous) were the solubility-limiting solid phase. The solubility decreased with crystallinity in the order of $AmCO_3OH(s) > AmCO_3OH{\cdot}0.5H_2O(s) > AmCO_3OH(cr)$. When $AmCO_3OH(cr)$, $AmCO_3OH{\cdot}0.5H_2O(s)$ and $Am(OH)_3(cr)$ solid phases were excluded, $Am_2(CO_3)_3(s)$, $AmCO_3OH(s)$ and $Am(OH)_3(am)$ appeared as solubility-limiting solid phases depending on the pH.

The Am concentrations in the filtrates were much higher than the solubility of $AmCO_3OH{:}0.5H_2O(s)$ (Fig. 8(a)) and slightly lower than that of $AmCO_3(OH)(s)$ (Fig. 8(b)). These values are much lower than those for $Am_2(CO_3)_3(s)$ alone (Fig. 8(b)). According to NEA-TDB, Vol. 5, $AmCO_3OH{\cdot}0.5H_2O(s)$, $AmCO_3OH(s)$, and $Am_2(CO_3)_3(s)$ are classified as hydrated crystalline $AmCO_3OH{\cdot}0.5H_2O$(cr, hyd), amorphous $AmCO_3OH$(am), and amorphous $Am_2(CO_3)_3$(am), respectively [2]. However, there are no selected thermodynamic data for dissolution of hydrated crystalline $Am_2(CO_3)_3{\cdot}xH_2O(s)$, which would be less soluble than the amorphous $Am_2(CO_3)_3$(am). As similar concentrations were observed in both Am ($(5.48 \pm 1.3)\times10^{-8}$ M) and Eu ($(6.08 \pm 0.05)\times10^{-8}$ M), formation of the hydrated crystalline $Am_2(CO_3)_3{\cdot}xH_2O(s)$ phase should be considered as in the case of Eu. More experimental data are required for Am–carbonate systems to better evaluate their solubility in natural water environments.

4. Conclusions

The solubilities of trivalent Sm, Eu, and Am were measured in synthetic KURT-DB3 groundwater, Syn-DB3, and evaluated in comparison with geochemical modeling results based on the ThermoChimie TDB. When $Ln_2(CO_3)_3{\cdot}xH_2O$(cr) (Ln = Sm, Eu) solid compounds were equilibrated in the Syn-DB3, the dissolved Sm and Eu concentrations were $(3.98 \pm 0.04) \times 10^{-8}$ and $(6.08 \pm 0.05)\times10^{-8}$ M at pH 8.19 and 8.26, respectively. These values were comparable to those of $Sm_2(CO_3)_3(s)$ and $Eu_2(CO_3)_3(s)$ as evaluated by geochemical modeling. XRD analysis before and after experiments confirmed that the crystallinities of the solid compounds of $Ln_2(CO_3)_3{\cdot}xH_2O$(cr) were maintained throughout the experiments. TRLFS results support the modeling results on aqueous Eu species, mixtures of $Eu(CO_3)^+$ and $Eu(CO_3)_2^-$, as dominant aqueous species in the Syn-DB3 condition. When Am solubility in Syn-DB3 was measured under over-saturation conditions, the aqueous Am concentrations converged to $(5.48 \pm 1.3)\times10^{-8}$ M under pH 8.45 ± 0.13 condition. This is comparable to the dissolved Eu concentrations in equilibration of $Eu_2(CO_3){\cdot}xH_2O$(cr). Our results show that more experimental data are required for Ln/An-carbonate systems, with careful characterization of the solid phases, to better evaluate their solubilities in domestic natural water systems.

Conflict of Interest

No potential conflict of interest relevant to this article was reported.

Acknowledgements

This study was supported by the Nuclear Research and Development Program of the National Research Foundation of Korea (Grant Nos. 2021M2E1A1085202 to iKNSF and 2022M2D2A1A02063990). Authors thank for analytical supports (ICP-OES, ICP-MS and XRD) of the Radioactive Material Chemical Analysis Section, KAERI (project no. 522330-24).

REFERENCES

[1] J.I. Kim, “Significance of Actinide Chemistry for the Long-Term Safety of Waste Disposal”, Nucl. Eng. Technol., 38(6), 459-482 (2006).

[2] R. Guillaumont, T. Fanghänel, J. Fuger, I. Grenthe, V. Neck, D. Palmer, and M.H. Rand, Update on the Chemical Thermodynamics of Uranium, Neptunium, Plutonium, Americium, and Technetium, 1st ed., Chemical Thermodynamics Vol. 5, Elsevier, Netherlands (2003).

[3] M. Hakanen, H. Ervanne, and E. Puukko. Safety Case for the Disposal of Spent Nuclear Fuel at Olkiluoto: Radionuclide Migration Parameters for the Geosphere, Posiva Oy Report, Posiva 2012-41 (2014).

[4] W. Runde, The Chemical Interactions of Actinides in the Environment, 26, 392, Los Alamos Scientific Laboratory, New Mexico (2000).

[5] H. Geckeis, J. Lützenkirchen, R. Polly, T. Rabung, and M. Schmidt, "Mineral–Water Interface Reactions of Actinides", Chem. Rev., 113(2), 1016-1062 (2013).

[6] H.K. Kim and H.R. Cho, "Evaluation of Americium Solubility in Synthesized Groundwater: Geochemical Modeling and Experimental Study at Over-Saturation Conditions", J. Nucl. Fuel Cycle Waste Technol., 20(4), 399-410 (2022).

[7] IAEA Nuclear Data Services. Accessed Mar. 27 2024. Available from: https://www-nds.iaea.org/.

[8] G.R. Choppin and E.N. Rizkalla, "Chapter 128 Solution Chemistry of Actinides and Lanthanides", in: Handbook on the Physics and Chemistry of Rare Earths, 18, 559-590 (1994).

[9] R.H. Byrne and E.R. Sholkovitz, "Chapter 158 Marine Chemistry and Geochemistry of the Lanthanides", in: Handbook on the Physics and Chemistry of Rare Earths, 23, 497-593 (1996).

[10] R.D. Shannon, "Revised Effective Ionic Radii and Systematic Studies of Interatomic Distances in Halides and Chalcogenides", Acta Crystallogr. A, 32(5), 751-767 (1976).

[11] V. Neck, T. Fanghaenel, and J.I. Kim. Aquatic Chemistry and Thermodynamic Modelling of Trivalent Actinides, Forschungszentrum Karlsruhe GmbH Technik und Umwelt Technical Report, FZKA--6110 (1998).

[12] I. Grenthe, X. Gaona, A.V. Plyasunov, L. Rao, W.H. Runde, B. Grambow, R.J.M. Konings, A.L. Smith, and E.E. Moore, Second Update on the Chemical Thermodynamics of Uranium, Neptunium, Plutonium, Americium, and Technetium, Chemical Thermodynamics Vol. 14, NEA No. 7500, OECD/ NEA Publishing, France (2020).

[13] H.R. Cho, H.K. Kim, H. Ju, J. Kim, and W. Um. Analysis of the Solubilities of Radioactive Materials in Oxidative Groundwater Conditions - Geochemical Modeling, Korea Atomic Energy Research Institute Technical Report, KAERI/TR-9156/2022 (2022).

[14] M. Grivé, L. Duro, E. Colàs, and E. Giffaut, "Thermodynamic Data Selection Applied to Radionuclides and Chemotoxic Elements: An Overview of the ThermoChimie-TDB", Appl. Geochem., 55, 85-94 (2015).

[15] E.C. Jung, H.R. Cho, M.H. Baik, H. Kim, and W. Cha, "Time-resolved Laser Fluorescence Spectroscopy of $UO_2(CO_3)_3^{4-}$", Dalton Trans., 43, 18831-18838 (2015).

[16] H.K. Kim, S. Choi, E.C. Jung, H.R. Cho, J.I. Yun, and W. Cha, "TRLFS Study of Hydrolyzed Eu(III) Species", J. Lumin., 202, 469-474 (2018).

[17] T. Kimura and G.R. Choppin, "Luminescence Study on Determination of the Hydration Number of Cm(III)", J. Alloys Compd., 213-214, 313-317 (1994).

[18] T. Kimura, R. Nagaishi, Y. Kato, and Z. Yoshida, "Luminescence Study on Solvation of Americium(III), Curium(III) and Several Lanthanide(III) Ions in Non-aqueous and Binary Mixed Solvents", Radiochim. Acta, 89(3), 125-130 (2001).

[19] K. Spahiu and J. Bruno. A Selected Thermodynamic Database for REE to be Used in HLNW Performance Assessment Exercises, Swedish Nuclear Fuel and Waste Management Co. Report, SKB TR 95-35 (1995).

[20] F.H. Firsching and J. Mohammadzadei, "Solubility Products of the Rare-Earth Carbonates", J. Chem. Eng. Data, 31(1), 40-42 (1986).

[21] L. Gordon, M.L. Salutsky, and H.H. Willard, Precipitation From Homogeneous Solution, John Wiley & Sons, Inc., New York (1959).

[22] K. Binnemans, “Interpretation of Europium(III) Spectra”, Coord. Chem. Rev., 295, 1-45 (2015).

[23] X. Tan, M. Fang, and X. Wang, “Sorption Speciation of Lanthanides/Actinides on Minerals by TRLFS, EXAFS and DFT Studies: A Review”, Molecules, 15(11), 8431-8468 (2010).

[24] G. Plancque, V. Moulin, P. Toulhoat, and C. Moulin, “Europium Speciation by Time-resolved Laser-induced Fluorescence”, Anal. Chim. Acta, 478(1), 11-22 (2003).

[25] J.I. Kim, R. Klenze, H. Wimmer, W. Runde, and W. Hauser, “A Study of the Carbonate Complexation of Cm(III) and Eu(III) by Time-resolved Laser Fluorescence Spectroscopy”, J. Alloys Compd., 213-214, 333-340 (1994).